

Monte Carlo model of sputtering and other ejection processes within a regolith

T.A. Cassidy*, R.E. Johnson

P.O. Box 3818, University of Virginia, Charlottesville, VA 22903-0818, USA

Received 15 November 2004; revised 16 February 2005

Available online 26 April 2005

Abstract

The ejection of atoms and molecules from a surface due to a flux of energetic particles has been studied for a variety of target materials and radiation types. We simulate these processes within a porous regolith using a Monte Carlo model. In doing so we assume that the surfaces of regolith grains behave like the surfaces of laboratory samples, where the results of an ejection event have been found to depend upon the energetic-particle angle of incidence and intrinsic properties of the target material. Total sputtering yields, sputter-product exit-angle distributions, and energy distributions are calculated for application to Solar System objects with emphasis on sodium ejection from the lunar surface. We find that the regolith yield is typically less than that from a laboratory surface made of the same material and depends on the sticking probability. The sputter-product exit-angle distribution from a porous regolith is found to be little altered by variation of the primary sputtering parameters, with the exception of nearly specular sputtering. The regolith grain shape has little effect on the total sputtering yield. The results are in rough agreement with an earlier analytic model [Johnson, R.E., 1989. Application of laboratory data to the sputtering of a planetary regolith. *Icarus* 78, 206–210]. The experimental results of Hapke and Cassidy [1978. Is the Moon really as smooth as a billiard ball? Remarks concerning recent models of sputter-fractionation on the lunar surface. *Geophys. Res. Lett.* 5 (4), 297–300] require a strongly forward-directed sputtering process, which may apply to a silicate with a low sputtering yield but not to the sputtering of ices by heavy ions. © 2005 Elsevier Inc. All rights reserved.

Keywords: Regoliths; Moon, surface; Surfaces, satellites; Atmospheres, composition

1. Introduction

The ejection of atoms and molecules from a surface due to a flux of ions, electrons or UV photons has been studied experimentally and computationally for a variety of target materials and radiation types. These treatments usually deal with relatively smooth target surfaces. Applying this knowledge to airless bodies in our Solar System is complicated by their surface structure. Meteor bombardment over millions or billions of years produces a regolith, a porous surface composed of grains formed by fracture and crater ejecta (Hapke and Cassidy, 1978; Hapke, 1986).

Regolith structure determines the distribution of incident angles to grain surfaces encountered by ions, which is im-

portant because experiments have shown that the sputtering yield depends on the incident angle. Further, the majority of sputter products encounter neighboring grains and do not directly escape to space (Hapke and Cassidy, 1978; Johnson, 1989). After encountering a grain the sputter products may then desorb, permanently stick, or even react. We have constructed a Monte Carlo model to simulate these processes and used it to show how the regolith affects the total yield, angular distribution, and energy distribution of sputtered products.

Regolith effects are relevant to the sputter fractionation of surface material and the supply of thin atmospheres on a number of Solar System objects, but are often not taken into account when modeling such atmospheres. This paper presents a comprehensive look at these issues. In addition, the results are relevant to the design of instruments for

* Corresponding author.

E-mail address: tac2z@virginia.edu (T.A. Cassidy).

measuring surface composition by sputtering (Elphic et al., 1991; Kirsch et al., 1997).

In this paper a Monte Carlo simulation is first described in which we follow the trajectories of incident particles and their sputter products within a regolith. The parameters used in the simulation were taken from literature on sputtering from laboratory surfaces. We calculate the effect of the porous regolith on the yield and on the angular and energy distributions of the ejecta. A similar program was used earlier by Hodges (1980) to study the transport of Ar across the lunar surface.

2. Model

In our simulation ions, electrons or photons are injected into the regolith one at a time. The incident particle, which we typically refer to as an ion, strikes a grain after traversing a randomly determined distance into the regolith as indicated in Fig. 1. This distance is, on average, the collisional mean free path, a quantity governed by the cross-sectional area of the grains and their density. Using a Poisson distribution, the ion's probability of striking a grain while traveling over a distance Δz is given by

$$1 - \exp\left(\frac{-\Delta z}{\lambda}\right), \quad (1)$$

where

$$\lambda = (n_g \sigma_g)^{-1}$$

is the collisional mean free path. n_g is the number of grains per unit volume and σ_g is the average cross-sectional area of the grains. The mean free path throughout the regolith is assumed to be isotropic. A distribution of grain sizes was also used, but that did not change the results presented here. Although we use a mean free path λ , all of the results presented below are independent of λ .

This independence is a consequence of the Poisson distribution and of the fact that the incident radiation and sputter products pass through the same distribution of regolith grains. These approximations are correct if the grain composition does not change with depth (down to at least a few mean free pathlengths) and for high porosity, porosity being the fraction of regolith volume *not* occupied by grains. At low porosities, as the regolith begins to resemble a flat surface, the Poisson distribution becomes less applicable. The results apply to a regolith where the inter-grain adhesive forces exceed average grain weight, resulting in a porous structure. Such a regolith was described by Hapke and van Horn (1963) as a “fairy castle,” in which in the upper few millimeters of soil can have a very low density and a dendritic structure. The method also can apply to a sand with a much lower porosity (Hapke and van Horn, 1963; Hapke and Cassidy, 1978) and to the sintered ice grains thought to be present in regions of Europa's surface (Grundy et al., 2001).

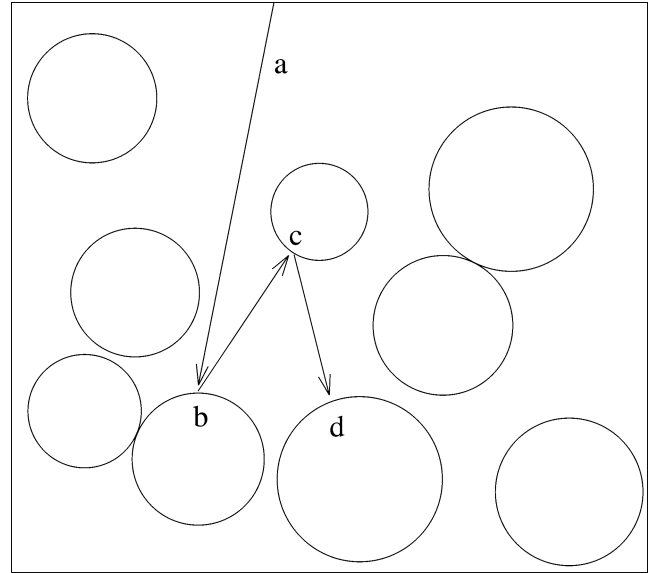


Fig. 1. A schematic view of the program. The spheres represent idealized regolith grains. (a) An ion or photon enters the regolith; (b) a sputter product is released; (c) the sputter product encounters a grain, and is then desorbed; (d) the desorbed sputter product is permanently adsorbed onto a grain.

Each time a grain is struck, the program randomly chooses a point on the grain where the impact occurs. This point determines the orientation of the surface, i.e. the angle of impact as suggested by Fig. 1. This probabilistic decision depends on the shape of the grain, which, in this simulation, is either a sphere, an ellipsoid, or a cube. The impact point on a grain surface is assumed to be locally equivalent to a “smooth” laboratory surface. This allows the use of data that describe sputtering yield as a function of $\theta_{g,i}$, the angle between the surface normal and incident ion trajectory, and the azimuthal angle $\phi_{g,i}$, which, when specified, is usually an angle between the incident ion trajectory and a crystal lattice direction. The ‘g, i’ subscript indicates that $\theta_{g,i}$ measures the angle between *incident* ion trajectory and the local surface normal on the *grain*. Angles used in this paper are defined in Table 1.

The quotation marks on “smooth” indicate that laboratory surfaces (and regolith grains) might not be perfectly smooth, but have submicroscopic relief. These features even vary between well-prepared lab samples and are generally not measured. Applying laboratory data is fraught with other uncertainties as well. For example, impurities can affect the sputter yields by altering the crystal structure (and hence altering collision cascades) (Bernardo et al., 1994) or by altering chemistry (Roth, 1983). Some of these difficulties are avoided by assuming that the regolith grains have amorphous surfaces, which results in the sputtering yield having no $\phi_{g,i}$ dependence (Betz and Wien, 1994; Carey and McDonnell, 1976). Therefore, for a given energy and incident ion species the sputtering yield is assumed to be a function of $\theta_{g,i}$ only. In addition, the steady state yields after long term irradiation are often the most relevant to Solar System surfaces.

Table 1
Definitions

Angle	Between	And
$\theta_{g,i}$	Incident ion traj.	Grain surface normal
$\phi_{g,i}$	Incident ion traj.	Vector parallel to grain surface
$\theta_{g,e}$	Sputter product traj.	Grain surface normal
$\phi_{g,e}$	Sputter product traj.	Vector parallel to surface
$\theta_{r,e}$	Sputter product traj.	Regolith surface normal
$\phi_{r,e}$	Sputter product traj.	Vector parallel to reg. surface
$\theta_{r,i}$	Incident ion traj.	Regolith surface normal
$\phi_{r,i}$	Incident ion traj.	Vector parallel to reg. surface

Each sputter product is given a “weight” which specifies the sputtering yield, the average number of particles sputtered per impact. The sputter yield from the grain surface is given by

$$Y_L(\theta_{g,i}) \approx \begin{cases} \frac{Y_L(0)}{\cos^n(\theta_{g,i})} & \text{if } \theta_{g,i} < \theta_c, \\ 0 & \text{if } \theta_{g,i} > \theta_c, \end{cases} \quad (2)$$

where θ_c is the cutoff angle, which is about 80° for a typical laboratory surface. This expression is commonly used to describe laboratory results for the yield, where $Y_L(0)$ is the sputtering yield for ions normally incident on a “smooth” laboratory surface, which depends upon incident ion energy and the material being sputtered (Sigmund, 1981). n and θ_c depend upon the sputtering mechanism and the submicroscopic relief of the surface (Johnson et al., 1987; Johnson, 1990). n is typically between 0 and 2, 1.6 being the most common for ions that significantly penetrate the grain surface (Johnson, 1990). Thus the sputtering yield increases as the incident ion trajectory moves away from normal except when $n = 0$, which applies roughly at very low velocities or to surfaces that are very rough at the submicroscopic scale. Jurac et al. (2001) considered the change in incident-angle dependence of the sputtering yield with ion energy and type in more detail for the sputtering of water ice grains in Saturn’s E-ring. In the following we use $n = 0, 1$ or 1.6.

Four cases are considered for the distribution in angle at which the sputter product leaves the grain surface. These distributions are not well measured for the materials of interest. The most common distribution used, sometimes called the Knudsen cosine law (Sigmund, 1981), is independent of incident ion angle $\theta_{g,i}$, and has the highest probability of emission at $\theta_{g,e} = 0$, the surface normal:

$$f(\cos(\theta_{g,e})) \approx 2 \cos(\theta_{g,e}), \quad (3)$$

where the subscript ‘g, e’ indicates measurement of the exit angle with respect to the local surface normal on the grain. This independence is a reflection of either an extensive cascade of collisions or energy deposition that can be treated as a “thermal” or “diffusive” spike (Johnson et al., 1989). In these cases the “memory” of the incident ion momentum is lost (Johnson, 1990). Equation (3) is herein referred to as the cosine law.

Two cases of forward-directed sputtering are considered, where the sputter products preferentially leave the surface

away from the incident beam direction. An example of such a process is “single-collision” sputtering, where a particle is directly ejected during the first few collisions following impact. The “memory” of the incident direction is not lost (Betz and Wien, 1994). This situation results from some combination of high target binding energy and low projectile momentum transfer, both of which inhibit the creation of extensive collision cascades (Hofer, 1991). As an extreme case, we first approximate forward-directed sputtering as specular:

$$\theta_{g,e} = \theta_{g,i}, \quad \phi_{g,e} = \phi_{g,i} + \pi. \quad (4)$$

Sputtering is more effectively at oblique incident angles, so Eq. (2) with $n = 1.6$ is still used. Johnson (1989) also used this as one approximation in his analytic model of regolith sputtering.

Surprisingly, large whole molecules ejected by fast heavy ions are primarily forward directed (Johnson et al., 1989). This is the “pressure pulse” regime of electronic sputtering. The analytical model of Johnson et al. (1989) predicts that $f(\cos(\theta_{g,e}))$ will have two peaks, one forward directed and one backward directed. Molecular-dynamics simulations and experiments (Fenyö et al., 1990) show that forward-directed sputter products dominate, so we use the forward-directed peak given by

$$\theta_{g,e} = \frac{\pi}{4} - \frac{\theta_{g,i}}{2}, \quad \phi_{g,e} = \phi_{g,i} + \pi. \quad (5)$$

The dependence of total sputtering yield on incident angle $\theta_{g,i}$ is again given by Eq. (2) with $n = 1.6$ (Johnson et al., 1989).

A third distribution applies when a molecular material is highly dissociated. In this case the small fragments come from depth and preferentially leave back along the incident ion direction (Johnson et al., 1989).

In all cases, the energy distribution of sputtered particles is assumed to be roughly independent of incident angle or exit angle. This is reasonable when the yield is large, as it is for the sputtering of the icy surfaces on the jovian satellites by heavy ions (Johnson, 1990). This is also used frequently for small yield cases (Sigmund, 1981), although that is a poor approximation.

After determining the sputter-product exit direction, sputter products are allowed to traverse the regolith until exiting the regolith surface or encountering another grain. Products encountering other grains may either permanently adhere or desorb. If they desorb, the exit-angle distribution with respect to the local grain normal is approximated by the cosine law [Eq. (3)] (Johnson, 2002; Hodges, 1980). The probability that a particular sputter product will not desorb is S , the sticking probability, a quantity that describes the affinity between an adsorbed sputter product and regolith grains. If $S = 1$ all sputter products that encounter a grain are permanently adsorbed onto that grain, and $S = 0$ implies that sputter products never stick permanently.

3. Results

We first discuss simulations with the parameter $S = 1$, which restricts us to ejecta that leave the regolith without encountering other grains. Then we assume $S < 1$ to include sputter products that encounter grains before leaving the regolith. These sputter products have undergone adsorption and desorption, and, in the process, have lost energy and memory of initial ejection direction. The difference in energy distributions between directly-sputtered and desorbed particles motivates this separation.

3.1. $S = 1$: Sputtering yield

The regolith sputtering yield, Y_R , is the average number of sputter products per incident ion that escape from the regolith. Results are presented in Tables 3 and 4 as the scaled sputtering yield $Y_R/Y_L(0)$, where $Y_L(0)$ is the yield at normal incidence on a “smooth” surface in Eq. (2). Definitions for the various sputter-yield related quantities are provided in Table 2.

In each calculation a distribution of incident ion angles with respect to the regolith surface normal is assumed. Results are given for a single flow direction, which here is always normal to the regolith surface ($\cos(\theta_{r,i}) = 1$), and “uniform” bombardment or isotropic incidence. For a sphere

in a flux of parallel-velocity ions, the average distribution of incident angles relative to the local surface normal is the same as for uniform bombardment:

$$f(\cos(\theta_{r,i})) = 2 \cos(\theta_{r,i}).$$

The percentage of sputter products that stick to other grains is given in the column under “percent retained” in Tables 3 and 4. The parameter n , defined in Eq. (2) determines the enhancement of the yield vs. incident angle as discussed above.

Two related results are given for comparison to $Y_R/Y_L(0)$. $Y_F/Y_L(0)$ gives the scaled sputtering yield that would be found if, in place of a regolith, the incident angle distribution impinges onto a flat “smooth” laboratory surface with the same material properties as the regolith grains. $Y_G/Y_L(0)$ is the scaled sputtering yield from a single isolated grain, like those in the E-ring of Saturn. In both cases the percent retained is, of course, zero.

In Table 3 the grains were assumed to be spherical, $S = 1$, and cosine law sputtering was used in Eq. (3). The third row of Table 3, for example, tells us that a regolith with the assumed properties and exposed to normally incident ion flux would have a scaled sputtering yield $Y_R/Y_L(0) \approx 0.64$. Removing adsorption due to regolith grains yields $Y_G/Y_L(0) \approx 2.5$. Comparing the two we find that 74% of the sputter products are retained by the regolith. As mentioned above, the yield resulting from uniform incidence onto a flat surface is equivalent to the yield resulting from a flow of parallel-velocity ions onto a sphere. From the last row in Table 3 it is seen that, for uniform incidence, the yield from a flat smooth surface is about 2.5 times the yield for normal incidence.

Table 4 presents results for specular sputtering [Eq. (4)], again using $n = 1.6$ in Eq. (2). It is seen, not surprisingly, that the effective yield from the regolith is further suppressed. That is, the percentage of sputter products permanently adsorbed onto regolith grains increases from $\approx 70\%$ to $\approx 90\%$.

We also carried out simulations assuming that the grains were all cubes or all ellipsoids. The grain orientations were randomized. We found that the results are not significantly altered by the change in grain shape. With use of cosine law sputtering, the yields $Y_R/Y_L(0)$ for cubic grains are slightly lower (at most 10%) and the percent retained is a slightly higher than for spherical-grain simulations (that otherwise use the same parameters). For forward-directed sputtering [Eqs. (4) and (5)], use of cubic grains results in slightly larger yields and slightly smaller percent retained as compared to the use of spherical grains.

The yields for prolate and oblate spheroid grains (a subset of ellipsoid shapes) depend on the ratio of the axial length c to the circular cross-section radius a . For cosine law sputtering, as c/a increases or decreases from unity ($c/a = 1$ corresponds to a sphere), the yield increases slightly. The yield from a regolith reaches a maximum of about 10% larger than the spherical-grain yields. At $c/a = 5$ and $1/5$, $Y_G/Y_L(0) = 3.1$ and 2.7 , respectively. For specular sputtering, use of oblate or prolate spheroids results in smaller

Table 2
Definitions

Y_R	Total yield from regolith
$Y_{R,des}$	Total yield of desorbed products
Y_G	Single-grain yield
Y_F	Yield from a laboratory surface

Table 3
Scaled sputtering yields^a: Cosine law emission and $S = 1$

n	Incidence	$Y_F/Y_L(0)$	$Y_G/Y_L(0)$	$Y_R/Y_L(0)$	Percent retained
0.0	Normal	1.0	1.0	0.29	70%
1.0	Normal	1.0	1.7	0.45	73%
1.6	Normal	1.0	2.5	0.64	74%
0.0	Uniform	1.0	1.0	0.30	69%
1.0	Uniform	1.7	1.7	0.49	70%
1.6	Uniform	2.5	2.5	0.71	72%

^a Computed with use of spherical grains and cosine law sputtering [Eq. (3)].

Table 4
Scaled sputtering yields^a: Forward-directed sputtering and $S = 1$

Exit-angle dist.	Incidence	$Y_F/Y_L(0)$	$Y_R/Y_L(0)$	Percent retained
Specular	Normal	1.0	0.19	92%
Specular	Uniform	2.5	0.32	87%
Pressure-pulse	Normal	1.0	0.52	79%
Pressure-pulse	Uniform	2.5	0.63	75%

^a Computed with use of the two forward-directed sputtering models [specular: Eq. (4), pressure pulse: Eq. (5)] spherical grains and $n = 1.6$ in Eq. (2).

yields (by about 30%). For pressure-pulse sputtering, use of spheroids results in slightly higher yields (about 10%).

For sputtering strongly peaked in the back direction, it was assumed that $n = 0$ in Eq. (2), although the sputter yield angular dependence has not been measured. The scaled yield ($Y_R/Y_L(0)$) was found to be about 0.5, with 50% retained, for all grain shapes and for both uniform and normal incidence. Because the sputter product is ejected along the path of the incident ion, the distance a sputter product must travel to exit the regolith is not affected by the ion incident angle ($\theta_{r,i}$) as it is for other types of sputtering.

3.2. $S = 1$: Exit-angle distributions

Fig. 2 shows the regolith exit-angle distribution $f(\cos(\theta_{r,e}))$. Data sets in Fig. 2 used cosine law sputtering [Eq. (3)] for the grain exit-angle distribution and $n = 1.6$ in Eq. (2). The smooth-surface distribution, which is just the cosine law, is what would be found if a laboratory surface

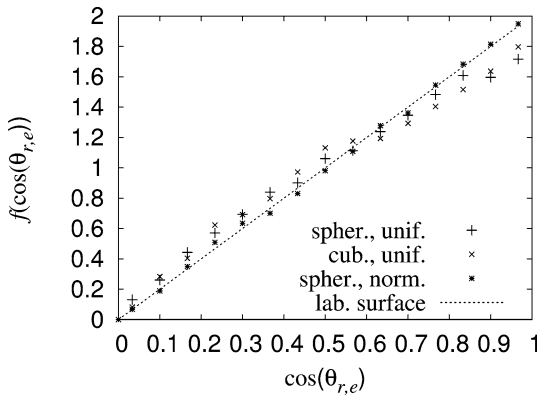


Fig. 2. The sputter-product exit-angle distributions from a regolith (data points) as compared to the exit-angle distributions for a smooth surface (dotted line). All four distributions are normalized to unity. Cosine law sputtering and $n = 1.6$ in Eq. (2) was used with combinations of cubic grains, spherical grains, uniform incidence, and normal incidence.

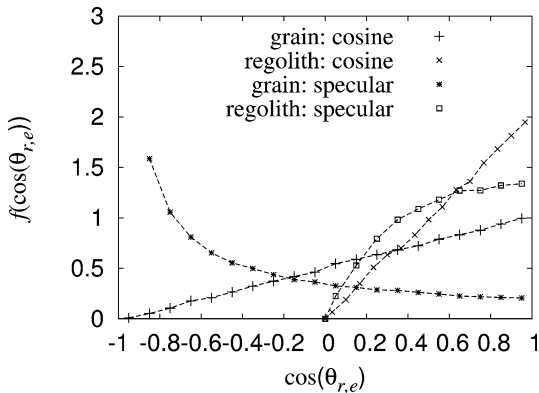


Fig. 3. Comparison of exit-angle distributions from a regolith with corresponding distributions due to a single grain (labeled “grain”). Spherical grains and normal incidence were used for all cases. The cosine law sputtering distribution is given by Eq. (3). Forward-directed specular sputtering is given by Eq. (4). All four distributions are normalized to unity; the single-grain yields $Y_R/Y_L(0)$ are much larger than the regolith yields.

were used. It is seen that the regolith exit-angle distributions are all, surprisingly, quite similar.

The curves labeled “grain” in Fig. 3 show exit-angle distributions from a single spherical grain without adsorption or desorption, i.e. all sputter products have been given a free path to the vacuum. Comparing this to the distributions from Fig. 2 demonstrates the effect of regolith absorption, which is to filter the ‘single grain’ distribution. As a trajectory within the regolith moves away from the regolith normal ($\cos(\theta_{r,e}) = 1$), the sputter product must travel farther to exit the regolith, and thus is more likely to be adsorbed.

Fig. 3 also shows distributions produced using forward-directed specular sputtering [Eq. (4)]. The regolith exit-angle distribution is relatively broad compared to the cosine law. As above, filtering by the regolith is still in effect, but relatively few sputter products are emitted toward the regolith normal. This is true of all three grain shapes, although for cubic grains and normal incidence the peak in the regolith normal direction ($\cos(\theta_{r,e}) = 1$) is stronger. The regolith angular distributions for pressure-pulse sputtering are similarly broad.

3.3. $S < 1$: Yields and angular distributions

We now consider sputter products that do not permanently stick when encountering grains. We do this by choosing S , the sticking probability, to be less than one. The column “ $Y_{R,des}/Y_L(0)$ ” in Table 5 shows the sputter yield due to desorbed sputter products only. The total sputter yield is given by

$$\frac{Y_R}{Y_L(0)} = \frac{Y_{R,des}}{Y_L(0)} + \frac{Y_R(S=1)}{Y_L(0)}, \quad (6)$$

where $Y_R/Y_L(0)$ is the net sputtering yield and $Y_R(S=1)/Y_L(0)$ is the sputtering yield due only to products that escape directly to the vacuum. The results in Table 5 and Fig. 4 were calculated using parameters from row 3 of Table 3, but with a varied sticking probability S . It is seen, not surprisingly, that the percent retained decreases as S decreases and that

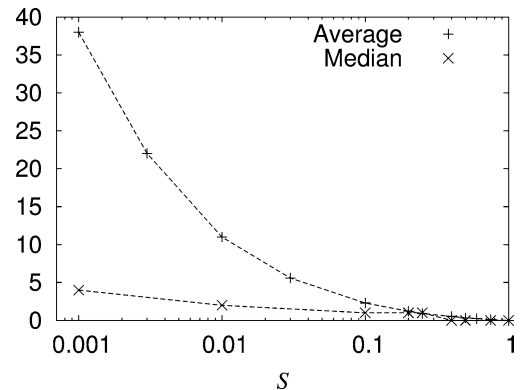


Fig. 4. Plot of data from Table 5: the average and median number of desorptions undergone by sputter products that escape the regolith, as a function of the sticking probability S .

Table 5
Scaled sputtering yields^a: Cosine law sputtering and $S \neq 1$

S	$Y_{R,des}/Y_L(0)$	$Y_R/Y_L(0)$	Percent retained
1.0	0.0	0.64	74%
0.5	0.16	0.80	68%
0.1	0.67	1.31	48%
0.01	1.35	1.99	21%
0.001	1.69	2.33	8%
0	1.86	2.5	0%

^a Computed with use of normal incidence, spherical grains, cosine law sputtering [Eq. (3)], and $n = 1.6$ in Eq. (2).

the scaled yield increases as S decreases. At $S = 0$ the total yield from the regolith $Y_R/Y_L(0)$ becomes equal to the single-grain yield discussed earlier.

a_{des} is defined as the average number of desorptions undergone by sputter products before leaving the regolith. m_{des} is the median number of desorptions undergone. Knowledge of a_{des} and m_{des} is useful in understanding processes such as the transport of neutral argon across the lunar surface (Hodges, 1980). Hodges (1980) approximates diffusion through a regolith as a random-walk process and shows that $a_{des} \rightarrow \infty$ as $S \rightarrow 0$. This divergence is suggested in our simulations, and we found that $m_{des} \rightarrow 5$ as $S \rightarrow 0$. At low S , a_{des} is skewed to large values since a few ejecta make it deep into the regolith before finally surfacing, although a majority of sputter products escape after a few collisions with grains.

These results for a_{des} and m_{des} are qualitatively similar for other regolith grain shapes and grain exit-angle distributions. The reason being that, since the desorption exit-angle distribution is always given by Eq. (3), a sputter product that encounters a grain while traveling upwards through the regolith is most likely to be desorbed downwards and vice-versa, irrespective of grain shape. This is true for any set of parameters.

It was also found that as $S \rightarrow 0$, the regolith exit-angle distributions approached the cosine law for any set of parameters. However, the sputter-product energy distributions will differ significantly from the $S = 1$ case as discussed below.

4. Comparisons

In (Johnson, 1989), the regolith sputter yield was estimated using an analytic model based on equations that describe light scattering in a regolith. The ‘single scattering’ limit for the light transport equations roughly corresponds to $S = 1$. The regolith was assumed to be composed of spherical grains and $n = 1.6$ in Eq. (2) was used. It was found that

$$Y_R \approx cY_L(0), \quad (7)$$

where c is between 0.4 and 1.0 depending on the exit-angle distribution. Tables 3 and 4 give somewhat smaller

yields, between 0.2 and 0.7. For the case of Table 3, row 6, $Y_R/Y_L(0) = 0.71$, whereas the analytical model in (Johnson, 1989) for roughly the same parameters gave a somewhat larger ratio, $Y_R/Y_L(0) = 0.85$. Similarly, for Table 4, row 2, $Y_R/Y_L(0) = 0.32$, while the analytic model gave $Y_R/Y_L(0) = 0.35$.

Hapke and Cassidy (1978) experimentally compared the total sputter yield from a macroscopic sphere and a powder made of the same material (basalt). Both were exposed to the same flux of 2 keV hydrogen ions (to reproduce solar wind exposure on Earth’s moon). The samples were then weighed to determine the sputter yield. They found that the sputter yield of the sphere was over ten times that of the powder, leading to the conclusion that over 90% of the sputter products were retained by the ‘regolith.’ Only the forward-directed specular sputtering [Eq. (4)] can reproduce such results in the Monte Carlo simulation. This was also the case for the analytic model (Johnson, 1989). All other models evaluated here limit retention to around 80% (using parameters similar to Table 3). Because protons incident on a silicate have a low sputter yield, the ejecta are likely to be forward directed (Hofer, 1991).

5. Applications

5.1. Energy distributions

Sputtering on the lunar surface is of particular interest to the authors, but energy distributions for relevant materials are sparse. The sputtering of Na_2SO_4 , a component of Io’s surface, provides a decent analogue as it has a low sputtering yield, more akin to minerals than ices. Wiens et al. (1997) measured the velocity distribution for a number of neutral sputter products resulting from the collisional-cascade sputtering of Na_2SO_4 by 3.5 keV Ar^+ ions. We will use ejected Na as an example. Their results are well approximated by the ‘planar binding’ sputter product energy distribution (Johnson, 1990) given by

$$f_p(E) = \frac{2UE}{(E+U)^3}, \quad (8)$$

where E is the sputter product energy, and the binding energy $U \approx 0.24$ eV, as found by a fit to their data. This energy distribution is assumed to be independent of incident ion direction and sputter-product exit angle (Wiens et al., 1997; Johnson, 1990).

As mentioned before, the regolith affects the energy distribution because some sputter products hit grains before leaving the regolith. We model this by assuming that the sputter products ‘fully accommodate’ or thermalize on regolith grains, that is, they take on the Maxwell flux distribution given by

$$f_m(E) = (E/(kT))^2 \exp(-E/kT), \quad (9)$$

where T is the regolith temperature.

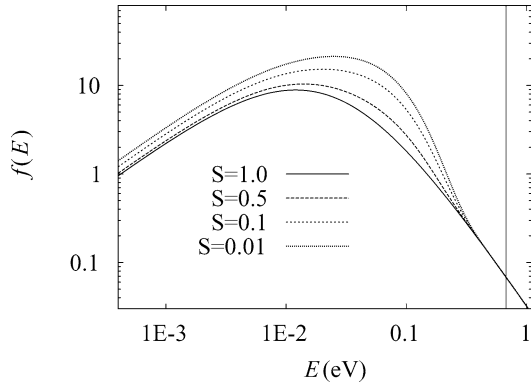


Fig. 5. The sputter-product energy distribution for various values of the sticking probability S . This distribution is a sum of two distributions; a measured distribution for sputter products and the Maxwell velocity distribution for 400 K. The vertical line indicates the escape energy of sodium at the Moon. These distributions are not normalized to unity, but rather to the scaled sputtering yields $Y_R/Y_L(0)$ at each S .

The energy distribution is described as a sum of a directly sputtered component [Eq. (8)] and a thermally accommodated component [Eq. (9)]:

$$f(E) = A[Y_{R,des}f_m(E) + Y_R(S=1)f_p(E)], \quad (10)$$

where A is a normalization constant. Fig. 5 gives the resulting velocity distribution for various sticking probabilities. The distributions in Fig. 5 are normalized to the scaled sputtering yield $Y_R/Y_L(0)$ for each S .

The relative contributions $Y_{R,des}$ and $Y_R(S=1)$ for f_m and f_p were determined by the Monte Carlo program (with results similar to Table 5). Uniform incidence, spherical grains, cosine law sputtering, and $n = 1.6$ in Eq. (2) were used in all cases. f_m was calculated for $T = 400$ K, which is approximately the maximum lunar temperature.

The distribution $S = 1$, described by the solid line, is the distribution reported by Wiens et al. (1997). It is due to sputter products that escape the regolith without encountering grains. The desorbed products are seen to increase in importance as S decreases. Such a combination of thermal and suprathermal energy distributions has been seen in the lunar atmosphere (Sprague et al., 1992). Based on sodium's energy of escape on the Moon, indicated by the vertical line, the amount of sputtered sodium that escapes is seen to be nearly independent of sticking probability, even at this high temperature. For the sputtering of ices by energetic heavy ions, the laboratory energy distributions peak at very low ejecta energies (e.g., Johnson, 1990) so that the effect of thermal accommodation in the regolith on the energy distribution of the ejecta is smaller than it is in Fig. 5.

5.2. Photon stimulated desorption of sodium

The Monte Carlo model described above was also used to calculate the effects of a regolith on the photon-stimulated desorption (PSD) of sodium from the lunar surface. We calculated the PSD yield from a porous regolith as a function of

solar zenith angle at local noon. The zenith angle is just the photon incident angle, and is the value used for $\theta_{r,i}$ in our model (see Table 1).

Yakshinskiy and Madey (2003) experimented with a lunar basalt sample and found that the yield of neutral sodium atoms due to ultraviolet photons is roughly proportional to the intensity of light reaching the grain surface and the surface concentration of sodium (for less than one monolayer of coverage). The yield also has a temperature dependence that fits an Arrhenius form over a temperature range of 100 to 470 K,

$$Y_{PSD} = CIX \exp(-E_A/kT), \quad (11)$$

where C is a constant, I is the intensity of ultraviolet photons, X is the sodium surface concentration, and the activation energy, E_A , was found to be about 20 meV for the lunar sample (Yakshinskiy and Madey, 2004).

Based on Clementine orbiter data, local noon temperature as a function of solar zenith angle i was reported by Lawson et al. (2000) as

$$T(i) \approx 380(\cos(i))^{(1/4)} \text{ K} \quad (12)$$

away from the poles ($i < 80^\circ$).

Yakshinskiy and Madey (2000) also measured the sticking probability of sodium onto SiO_2 , an analogue to lunar soil, as a function of temperature. Specifically, they measured the probability that a sodium atom adsorbed at 250 K would later desorb when the SiO_2 substrate was heated. We assume those measured values approximate the sticking probability in the present calculation, which is reasonable when the PSD products fully accommodate on regolith grains. Yakshinskiy and Madey (2000) measured the sodium sticking probability at 3 temperatures, which were interpolated for the present calculation. Given $T(i)$, the sticking probability varies between 0.25 (at 0° zenith angle) and 0.5 (at 80° zenith angle).

The PSD product exit-angle distribution with respect to the local grain normal is assumed to be given by the cosine distribution [Eq. (3)]. Since the photon incident-angle dependence of PSD has not been measured, we calculated two cases: $n = 0$ and $n = 1$ in Eq. (2), as examples.

Fig. 6 compares the sodium yield from a regolith-covered Moon to that of an imaginary smooth moon. The yield in Fig. 6 has been divided by the smooth surface yield at 0° solar zenith angle. The smooth-moon yield is given by

$$Y_{\text{smooth}}(i) = A \cos(i) Y_{PSD}(T(i)), \quad (13)$$

where i is the zenith angle and A is a constant and $\cos(i)$ is proportional to the intensity of sunlight. It is assumed that the surface concentration of sodium, X , is a constant over the lunar surface. For the present conditions Y_{PSD} varies by about 30% between 0° and 80° zenith angle. Thus the dominant variation in $Y_{\text{smooth}}(i)$ is given by $\cos(i)$.

The yield for the regolith-covered Moon can be thought of as $Y_{\text{smooth}}(i)$ times another factor that accounts for the

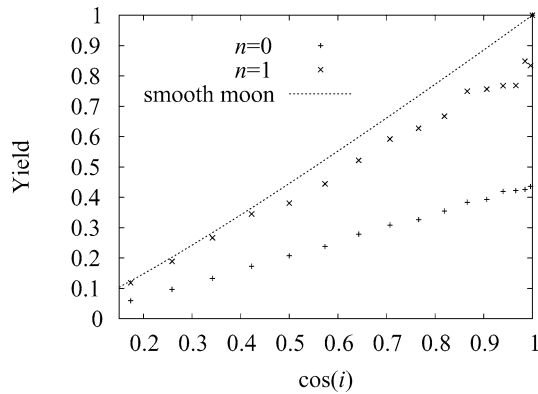


Fig. 6. The yield of sodium resulting from photon-stimulated desorption on the Moon as a function of solar zenith angle (i). The data labeled “ $n = 0$ ” and “ $n = 1$ ” were calculated for a regolith-covered Moon. n is a parameter in Eq. (2). The smooth-moon yield is given by Eq. (13).

effect of a regolith, $Y_{\text{filter}}(i)$. The regolith effects are determined by the sticking coefficient, which is a function of temperature, and photon incident angle. For $n = 0$, $Y_{\text{filter}}(i)$ varies between 0.44 at 0° zenith angle and 0.35 at 80° . Thus the dominant variation in regolith-covered Moon PSD yield is also $\cos(i)$ (see Fig. 6).

The neutral sodium column density can be estimated as $[\langle t \rangle(i)][Y(i)]$, where $Y(i)$ is the PSD yield given above and $\langle t \rangle(i)$ is the average time an ejected particle spends above the Moon’s surface in a ballistic orbit (Johnson, 1990). $\langle t \rangle(i)$ depends upon the distribution in energy, which depends upon the fraction of PSD products that thermalize on regolith grains. Thermalized ejecta are assumed to have the Maxwellian distribution for the energy [Eq. (9)], and directly ejected PSD products have a “suprathermal” distribution, with the same average energy as a 900 K Maxwellian (Yakshinskiy and Madey, 2004). The column density was found to be roughly proportional to $\cos(i)$ for both $n = 1$ and $n = 0$ because $Y(i)$ varies as $\cos(i)$ (as shown above), and $\langle t \rangle(i)$ is roughly constant over a wide range of i .

Sprague et al. (1992) observed a cosine dependence for the suprathermal component of the lunar sodium atmosphere. The observed sodium was, however, more energetic than the photon-desorbed sodium measured by Yakshinskiy and Madey (2004). Other observations suggest that the column density of sodium in the lunar atmosphere varies as $\cos^2(i)$ (Killen and Ip, 1999). Reproducing this dependence may require that the sodium concentration in the exposed layer varies with i (Potter et al., 2000), and consideration of other sources such as impact vaporization (Sprague et al., 1998).

6. Conclusions

A considerable amount of laboratory data on the sputtering of solids relevant to Solar System surfaces has been accumulated. However, the application of this data to sputtering of objects in the Solar System is often not straight for-

ward. Here we consider the application to individual grains, such as those in Saturn’s E-ring (Jurac et al., 2001), and to grains in a regolith on a planetary surface (Johnson, 1989). We examine the effect of sticking of ejecta to neighboring grains on the sputtering rate and on the angular distribution of the ejecta. We also consider the effect of thermal accommodation and subsequent desorption on the energy distribution of the ejecta. Because the sticking coefficients can differ between species ejected from the same surface, the relative yields from a planetary surface can differ considerably from the relative laboratory yields. This is the case for the ejection of O_2 ($S \approx 0$) and H_2O ($S \approx 1$) from Europa’s icy surface (Shematovich et al., 2003; Johnson et al., 2004). Assuming both yields are described by $n \approx 1.6$ in Eq. (2) and a cosine law exit angle distribution [Eq. (3)], the O_2 yield is from Table 5 ≈ 2.5 times that at normal incidence, whereas the H_2O yield from the regolith based on Table 3 is ≈ 0.71 times the that at normal incidence. Therefore, the $\text{O}_2/\text{H}_2\text{O}$ ratio is about 3.5 times the laboratory ratio. In non-ice regions this ratio can change and the oxygen might react on the grains (Shematovich et al., 2003). Therefore the regolith can significantly modify the relative populations of atmospheric species and their spatial distributions across the surface. This must be accounted for in describing Europa’s atmosphere. In a similar way the results in Tables 3–5 can also be used to determine the effect of sticking in the regolith on sputter fractionation of a planetary surface.

Whereas the sputtering rate of an individual grain in a uniform plasma is, typically, enhanced relative to that for normal incidence on a laboratory surface, the yield from a porous regolith is often reduced. The size of the reduction can be large but depends on the angular distribution of the ejecta from the surface of grains in the regolith, with the largest reductions occurring for forward-directed ejections. Here we find somewhat larger reductions than those obtained from an earlier analytic model (Johnson, 1989). We also find that the size of the reduction is not very sensitive to grain shape and does not depend on the porosity as long as the expression in Eq. (1) applies over the penetration range of the incident radiation. The sputter-product exit-angle distribution is similarly insensitive, and is given by the cosine law for a wide variety of model parameters.

The very large reduction in the yield found experimentally by Hapke and Cassidy (1978) is shown to apply when the ejecta is highly forward directed, which may be the case for the sputtering of a silicate by keV protons (Betz and Wien, 1994). The enhancement in the yield from a single grain (≈ 2.5 based on Table 3) is roughly consistent with the calculations of Jurac et al. (2001) for ice grains. However, the procedure suggested earlier for ices (Johnson, 1989), in which Y_R is assumed to be about equal to $Y_L(0)$ underestimates the regolith reduction unless $S \approx 0.5$ for the models considered here. Finally, we calculated the column density of PSD-derived neutral sodium in the lunar atmosphere as a function of latitude, and found that including a regolith modifies the source strength but not the dependence on latitude.

Acknowledgments

This work was supported by a grant from NASA's Geology and Geophysics Program and the NSF Astronomy Program.

References

- Bernardo, D.N., Bhatia, R., Garrison, B.J., 1994. keV particle bombardment of solids: Molecular dynamics simulations and beyond. *Comput. Phys. Commun.* 80, 259–273.
- Betz, G., Wien, K., 1994. Energy and angular distributions of sputtered particles. *Int. J. Mass Spectrom. Ion Process.* 140, 1–110.
- Carey, W.C., McDonnell, J.A., 1976. Lunar surface sputter erosion: A Monte Carlo approach to microcrater erosion and sputter redeposition. *Proc. Lunar Sci. Conf.* 7, 913–926.
- Elphic, R.C., III, H.O.F., Barraclough, B.L., McComas, D.J., Paffett, M.T., Vaniman, D.T., Heiken, G., 1991. Lunar surface composition and solar-wind induced secondary ion mass spectrometry. *Geophys. Res. Lett.* 18 (11), 2165–2168.
- Fenyő, D., Sundqvist, B.U.R., Karlsson, B.R., Johnson, R.E., 1990. Molecular-dynamics study of electronic sputtering of large organic molecules. *Phys. Rev. B* 42 (4), 1895–1902.
- Grundy, W.M., Spencer, J.R., Buie, M.W., 2001. Thermal inertia of Europa's H₂O ice surface component. *Bull. Am. Astron. Soc.* 33. Session 47.
- Hapke, B., 1986. On the sputter alteration of regoliths of outer Solar System bodies. *Icarus* 66, 270–279.
- Hapke, B., Cassidy, W., 1978. April 1978. Is the Moon really as smooth as a billiard ball? Remarks concerning recent models of sputter-fractionation on the lunar surface. *Geophys. Res. Lett.* 5 (4), 297–300.
- Hapke, B., van Horn, H., 1963. Photometric studies of complex surfaces, with applications to the Moon. *J. Geophys. Res.* 68, 4545–4570.
- Hodges, R.R., 1980. Lunar cold traps and their influence on argon-40. *Proc. Lunar Sci. Conf.* 11, 2463–2477.
- Hofer, W.O., 1991. Angular, energy, and mass distribution of sputtered particles. In: Behrisch, R., Wittmaack, K. (Eds.), *Topics in Applied Physics*. In: *Sputtering by Particle Bombardment III*, vol. 64. Springer-Verlag, Berlin. ch. 2.
- Johnson, R.E., 1989. Application of laboratory data to the sputtering of a planetary regolith. *Icarus* 78, 206–210.
- Johnson, R.E., 1990. *Energetic Charged-Particle Interactions with Atmospheres and Surfaces*. Springer-Verlag, Berlin.
- Johnson, R.E., 2002. Surface boundary layer atmospheres. In: Mendillo, M., Nagy, A., Waite, J.H. (Eds.), *Geophysical Monograph Series*. In: *Atmospheres in the Solar System*, vol. 130. American Geophysical Union, Washington, DC, pp. 203–219.
- Johnson, R.E., Carlson, R.W., Cooper, J.W., Paranicas, C., Moore, M.H., Wong, M., 2004. *Jupiter—The Planet, Satellites, and Magnetosphere*. Cambridge University Press. In press.
- Johnson, R.E., Sundqvist, B., Hakansson, P., Hedin, A., Salehpour, M., Save, G., 1987. Incident angle dependence of electronic desorption and sputtering by energetic ions. *Surface Sci.* 179, 187–198.
- Johnson, R.E., Sundqvist, B.U.R., Hedin, A., Fenyő, D., 1989. Sputtering by fast ions based on a sum of impulses. *Phys. Rev. B* 40, 49–53.
- Jurac, S., Johnson, R.E., Richardson, J.D., 2001. Saturn's E ring and production of the neutral torus. *Icarus* 149, 384–396.
- Killen, R.M., Ip, W., 1999. The surface-bounded atmospheres of mercury and the Moon. *Rev. Geophys.* 37 (3), 361–406.
- Kirsch, E., Wilken, B., Gloeckler, G., Galvin, A.B., Mall, U., Hovestadt, D., 1997. Comparison of lunar and terrestrial ion measurements obtained by the wind and geotail spacecraft outside and inside the Earth's magnetosphere. *Adv. Space Res.* 20, 845–849.
- Lawson, S.L., Jakosky, B.M., Park, H., Mellon, M.T., 2000. Brightness temperatures of the lunar surface: Calibration and global analysis of the Clementine long-wave infrared camera data. *J. Geophys. Res.* 105 (14), 4273–4290.
- Potter, A.E., Killen, R.M., Morgan, T.H., 2000. Variation of lunar sodium during passage of the Moon through the Earth's magnetotail. *J. Geophys. Res.* 105, 15,073–15,084.
- Roth, J., 1983. Chemical sputtering. In: Behrisch, R. (Ed.), *Topics in Applied Physics*. In: *Sputtering by Particle Bombardment II*, vol. 52. Springer-Verlag, Berlin. ch. 3.
- Shematovich, V., Johnson, R.E., Cooper, J.F., Wong, M.C., 2003. Supply of trans-Europa Neutral Torus by the Surface-bounded Atmosphere of Europa. *AGU Fall Meeting Abstracts*, B248+.
- Sigmund, P., 1981. Sputtering by ion bombardment: Theoretical concepts. In: Behrisch, R. (Ed.), *Topics in Applied Physics*. In: *Sputtering by Particle Bombardment I*, vol. 47. Springer-Verlag, Berlin. ch. 2.
- Sprague, A.L., Hunten, D.M., Kozlowski, R.W.H., Grosse, F.A., Hill, R.E., Morris, R.L., 1998. Observations of sodium in the lunar atmosphere during International Lunar Atmosphere Week, 1995. *Icarus* 131, 372–381.
- Sprague, A.L., Kozlowski, R.W.H., Hunten, D.M., Wells, W.K., Grosse, F.A., 1992. The sodium and potassium atmosphere of the Moon and its interaction with the surface. *Icarus* 96, 27–42.
- Wiens, R.C., Burnett, D.S., Calaway, W.F., Hansen, C.S., Lykke, K.R., Pellin, M.J., 1997. Sputtering products of sodium sulfate: Implications for Io's surface and for sodium-bearing molecules in the Io torus. *Icarus* 128, 386–397.
- Yakshinskiy, B.V., Madey, T.E., 2000. Thermal desorption of sodium atoms from thin SiO₂ films. *Surf. Rev. Lett.* 7, 75–87.
- Yakshinskiy, B.V., Madey, T.E., 2003. DIET of alkali atoms from mineral surfaces. *Surf. Sci.* 528, 54–59.
- Yakshinskiy, B.V., Madey, T.E., 2004. Photon-stimulated desorption of Na from a lunar sample: Temperature-dependent effects. *Icarus* 168, 53–59.